Available online at www.sciencedirect.com

ScienceDirect

Ceramics International 40 (2014) 4009–4018

CERAMICS INTERNATIONAL

www.elsevier.com/locate/ceramint

The dependence of the photocatalytic activity of TiO_2/carbon nanotubes nanocomposites on the modification of the carbon nanotubes

Veljko R. Djokić[a,*], Aleksandar D. Marinković[a], Ovidiu Ersen[b], Petar S. Uskoković[a], Rada D. Petrović[a], Velimir R. Radmilović[a,c], Djordje T. Janaćković[a]

[a]*Faculty of Technology and Metallurgy, University of Belgrade, Karnegijeva 4, 11120 Belgrade, Serbia*
[b]*Institut de Physique et Chimie des Matériaux de Strasbourg (IPCMS), UMR CNRS–Université de Strasbourg 7504, 23, rue du Loess, BP 43, F-67034 Strasbourg Cedex 2, France*
[c]*Nanotechnology and Functional Materials Center, Faculty of Technology and Metallurgy, University of Belgrade, Karnegijeva 4, 11120 Belgrade, Serbia*

Received 13 June 2013; accepted 10 August 2013
Available online 19 August 2013

Abstract

Nanostructural TiO_2/modified multi-wall carbon nanotubes photocatalysts were prepared by hydrolysis of Ti(*iso*-$OC_3H_7)_4$ providing chemical bonding of anatase TiO_2 nanoparticles onto oxidized- or amino-functionalized multi-wall carbon nanotubes (MWCNT). The processes of functionalization of the MWCNT and the deposition of TiO_2 influence the photocatalytic activity of the synthesized nanocomposites. The phase composition, crystallite size, and the structural and surface properties of the obtained TiO_2/modified-MWCNT nanocomposite were analyzed from XRD, FEG-SEM, TEM/HRTEM and FTIR data, as well low temperature N_2 adsorption. In the photocatalytic study, the TiO_2/oxidized-MWCNT catalyst showed the highest and the TiO_2/amino functionalized-MWCNT catalysts somewhat lower degradation rates, indicating that the enhancement of photocatalysis was supported by the more effective electron transfer properties of the oxygen- than amino-containing functional groups, which support the efficient charge transportation and separation of the photogenerated electron-hole pairs.

Keywords: A. Sol–gel processes; B. Nanocomposites; D. TiO_2; Carbon nanotubes; Photocatalysis

1. Introduction

Due to its outstanding physical and chemical properties, and especially photocatalytic activity, titanium dioxide (TiO_2) is one of the most studied semiconductor materials in fields of environmental protection and renewable energy sources. In the last four decades, much effort has been invested in research related to improving the photocatalytic activity of TiO_2 and its possible practical applications. Generally, in order to ensure a high photocatalytic activity, it is necessary to synthesize TiO_2 that, in addition to a large specific surface area, porosity and crystallinity, has an exceptional ability for more effective charge separation, *i.e.*, suppression of electron/hole recombination [1–5].

Pristine nanomaterials, *i.e.*, carbon nanotubes (CNT), are suitable preferentially for fundamental studies, but the vast number of their applications require their integration into composite structures. Improvement of the photocatalytic activity of TiO_2 was achieved by synthesis of composite materials based on the coupling of titania and functional nanostructured carbon materials. Special attention was devoted to CNT due to their chemical stability, unique structures, remarkable electron-transfer and adsorption, as well as their mechanical and thermal properties. In this way, CNT as photocatalysts carriers increased the separation and migration of photogenerated electrons and holes, prompting the creation of excess holes in the valence band, while the excited electrons moved from the conduction band of TiO_2 to the electron-accepting surface of the carbon

*Corresponding author. Tel.: +381 64 270 1090; fax: +381 11 3370 387.
E-mail addresses: vdjokic@tmf.bg.ac.rs, djokicveljko@yahoo.com (V.R. Djokić).

0272-8842/$ - see front matter © 2013 Elsevier Ltd and Techna Group S.r.l. All rights reserved.
http://dx.doi.org/10.1016/j.ceramint.2013.08.052

nanotubes. In addition, the relatively high specific surface area of CNT leads to an increase in the number of active sites for adsorption on the surface of TiO_2/CNT nanocomposites. Thus, CNT in a composite with TiO_2 have, at least, the dual effect of improving the photocatalytic activity by: (i) reducing the recombination of photogenerated electron/hole pairs by increasing their separation and (ii) increasing the specific surface area, *i.e.*, the number of active sites for the adsorption of the pollutants to be photocatalytically degraded [4,6,7].

However, the application of CNT was greatly hampered by their poor dispersion in solvents due to strong interactions between the nanotubes, which lead to the formation of sparingly soluble aggregates. CNT functionalization was found to be an effective method to overcome the solubility limitations, reactivity with respect to different modification agents, and to provide homogeneous distributions in a variety of mediums. One of the most common functionalization methods is the oxidative treatment of carbon nanotubes. After oxidative treatment, the CNT are shortened and mostly opened at the end, and oxygen-containing functional groups are unevenly distributed on surface, changing their surface properties and providing numerous sites for TiO_2 bonding [8]. A covalent or non-covalent modification of carbon nanotubes usually follows the oxidation step. The covalent modifications of the side-wall of CNT have been described in detail in several review articles [9,10]. In principle, major approaches comprise: (i) amidation or esterification of carboxylated CNT and (ii) side-wall covalent attachment of functional groups directly to pristine CNT. Among them, amino-functionalized CNT have high reactivity, and can react with many functionalities, such as different Ti-precursors [11]. The introduction of functional groups cause changes in the physical and electronic properties of nanotubes, providing a crucial prerequisite for improvement of the electron transport properties at titania/CNT interface, *i.e.*, photocatalytic performances, of the obtained hybrid materials [4,6,11–13].

The electronic properties of MWCNT depend on their structure and covalent functionalization, which affects their semiconducting and conducting properties. Despite the theoretical assumption that electron transport may be expected through both the outer and inner shells of multi-wall carbon nanotube (MWCNT), it was found that electron transport at low energies was mainly achieved through the outer surface of MWCNT. Improved electronic properties are highly desirable in the fabrication of supercapacitor, photovoltaic, nanoelectronic devices, transistors, high frequency nanoelectronics, storage media, field emission and nanoscale array fabrications [11,12].

A comparative examination of the electrochemical behavior of oxidized and ethylenediamine-modified MWCNT by cyclic voltammetry and electrochemical impedance spectroscopy confirmed that the existing oxygen-containing functionalities were responsible for the rapid electron transfer on the o-MWCNT surface. Amino-modification of the o-MWCNT, *via* oxygen containing groups, led to a slight decrease in the conductivity of the layer, the charge transfer properties, *i.e.*, reduced rate of electron transfer between the MWCNT and solution species, and the apparent capacitance [14,15].

The synthesis of high performance photocatalysts demands the design of such processes that could provide a MWCNT product with a surface containing chemical functionalities that possess high affinity and surface bonding specificity towards TiO_2. With this in mind, the synthesis of TiO_2/modified MWCNT at different ratios MWCNT/Ti(IV) isopropoxide precursor was performed to study the effect of the functionalization method on the crystallinity, morphology and photocatalytic activity in the photo-activated degradation reaction of the textile dye C.I. Reactive Orange 16 that has a detrimental impact when discharged untreated into the environment (Fig. 1).

2. Materials and methods

2.1. Preparation of the photocatalysts

MWCNT (95+ %, Aldrich), prepared by a chemical vapor deposition method, were used as received without purification. Titanium(IV) isopropoxide (98%, Ti(*iso*-$OC_3H_7)_4$, Aldrich), propan-2-ol, absolute ethanol and ethylenediamine (EDA, 99%, Fluka), 1,4-phenylene-diamine (PDA, 99%, Fluka), *N*, *N*-di-isopropylethylamine (DIEA, 99%, Sigma), *O*-(7-aza-benzotriazol-1-yl)-*N*,*N*,*N*′,*N*′-tetra-methyluroniumhexa-fluoro-phosphate (*N*-HATU, 98%, Fluka), concentrated sulfuric (H_2SO_4, 98%, Fluka) and nitric (HNO_3, 99%, Fluka) acid and methanol (Fluka, *p.a.*) were used as received. Millipore deionized water (DW; 18 MΩ cm resistivity) was used for sample washing and solution preparation. Dimethylformamide (DMF, 99.8%, Fluka) was purified and dried to remove any trace impurities and water [14,16].

2.1.1. Oxidation of MWCNT

Raw-MWCNT (480 mg) were dispersed in 520 ml of a (3:1 v/v) mixture of concentrated H_2SO_4 and HNO_3 acid, respectively, and sonicated for 3 h at 40 °C. After cooling to room temperature, the dispersion of the oxidized MWCNT (o-MWCNT) were added drop-wise to 1300 ml of cold DW water, and vacuum-filtered through a 0.05 μm pore size poly (tetrafluoroethylene) (PTFE) membrane filter. The filtrant was washed with DW water until pH was neutral. The sample was then dried in a vacuum oven at 80 °C for 8 h [16].

2.1.2. Functionalization of o-MWCNT with amines

o-MWCNT (160 mg) were dispersed in 95 ml of the liquid amine (EDA) for 10 min. The coupling agent *N*-HATU (12.8 mg) was then added, and dispersion was sonicated for 4 h at 40 °C

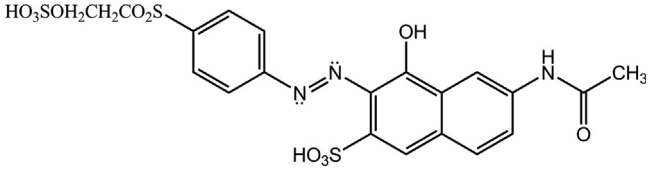

Fig. 1. The structure of C.I. Reactive Orange 16.

[16]. In the case of the solid amine (PDA), a mixture of 160 mg o-MWCNT, 12.8 mg *N*-HATU, 16 μl DIEA (the molar ratio *N*-HATU:DIEA was 1:3) and 4.8 ml anhydrous DMF was prepared in order to enhance activation of carboxyl groups by DIEA [14]. After activation for 15 min, PDA dissolved in anhydrous DMF (32 g PDA/160 ml DMF) was added into the reaction mixture and sonicated for 4 h at 40 °C. The product was diluted with 480 ml of methanol, vacuum-filtered (0.05 μm PTFE membrane) and washed extensively with excess methanol. The amino-functionalized MWCNT (EDA: e-MWCNT, and PDA: p-MWCNT) were dried in a vacuum oven at 60 °C for 8 h, and stored in a desiccator.

2.1.3. Synthesis of the TiO_2/MWCNT nanocomposites

In a three-necked flask (50 cm^3) equipped with a condenser and thermometer, 160 mg o-MWCNT, 13.6 cm^3 2-propanol and 2, 3, 4, 5, 6 or 8 cm^3 Ti(*iso*-$OC_3H_7)_4$ were added under magnetic stirring. Reaction mixture was heated at 80 °C for 7 h under moderate mixing (150 rpm), and oil-bath was removed, and mixing was continued, for additional 60 min providing reaction mixture to attain room temperature. After completion of the reaction, the obtained grayish/black TiO_2/o-MWCNT dispersion was vacuum-filtered (0.05 μm PTFE membrane) and washed with ample deionized water. After drying at 70 °C for 24 h, the material was ground to a fine powder and calcined at 400 °C for 2 h. The TiO_2/raw-, TiO_2/e- and TiO_2/p-MWCNT photocatalysts were prepared using the optimal ratio found for the preparation of the TiO_2/o-MWCNT photocatalyst. Additionally, pure TiO_2 (TiO_2-blank) was prepared by an analogous procedure but in the absence of MWCNT, and used in a comparative photocatalytic study.

2.2. Characterization

The specific surface area and pore volume of the samples were measured using an accelerated surface area and porosimetry system – ASAP 2020 (Micromeritics, USA). The X-ray diffraction (XRD) data were obtained using a BRUKER D8 ADVANCE with a Vario 1 focusing primary monochromator ($Cu_{k\alpha 1}$ radiation, $\lambda = 1.54059$ Å). The crystallite size of the anatase, D, was determined according to the Scherrer Equation:

$$D = K\lambda/(\beta \cos\ \theta)$$

where λ is the wavelength of the X-ray radiation ($\lambda = 1.54059$ Å), K is the Scherrer constant ($K = 0.9$), θ is the angle of the characteristic X-ray diffraction peak ($\theta = 12.65°$) and β is the full-width-at-half-maximum-height of the anatase (101) plane (in radians). Scanning electron microscopy (FEG-SEM) was performed with a field emission gun TESCAN MIRA3 XMU electron microscope. Conventional transmission electron microscopy (CTEM) was performed using an AEM JEOL 200CX microscope at 200 kV, and high resolution transmission electron microscopy (HRTEM) using a TEAM0.5 aberration corrected electron microscope operated at 80 kV, below the threshold of knock-on damage of the CNT [17]. The atomic compositions of the obtained materials were determined by electron energy-loss spectroscopy (EELS) in the scanning TEM (STEM) mode. The Boehm method [18] was applied for the determination of type and quantity of functional groups present on the surface of the oxidized and amino-functionalized MWCNT. Fourier-transform infrared (FTIR) spectra were recorded in the transmission mode using a BOMEM (Hartmann&Braun) spectrometer.

2.3. Photocatalytic activity

The photocatalytic decomposition of the textile dye C.I. Reactive Orange 16 (CI RO 16; Bezema) (Fig. 1) was followed by measuring the decrease of the absorbance of an aqueous dye solution (50 mg dm^{-3}) in the presence of the synthesized photocatalysts (50 mg in 25.0 cm^3 of solution). The dispersions were mixed in the dark for 30 min in order to establish the adsorption/desorption equilibrium and then illuminated with UV-A light using a Philips 125 W lamp with an intensity of 12.7 mW/cm^2. Aliquots (3.0 cm^3) were taken and separated from the photocatalysts by filtration through a 0.2 μm poly(vinylidene fluoride) (PVDF) syringe filter (Whatman), and used for the determination of time-dependent change of dye concentration using a Shimadzu 1800 UV–vis spectrophotometer. The light irradiation intensity was measured by a UVX Digital Ultraviolet Intensity Meter (Cole-Parmer, USA; Model: 97-0015-02(UVX)) using a 365 nm sensor (97-0016-02 (UVX36)). The durability of all nanocomposite catalysts was checked in five consecutive cycles. After each cycle, the catalyst was recovered by centrifugation, washed with ample DI water, dried at 80 °C, and reused in the next degradation cycle.

3. Results and discussion

The nanocomposite photocatalysts were prepared by a two-step process, functionalization of the MWCNT (consecutive processes of oxidation and amino modification) and precipitation of TiO_2, providing chemical bonding of TiO_2 deposit on the MWCNT support. To perform crystallization of precipitated $Ti(OH)_4$, a low temperature heat treatment in air was performed to prevent the decomposition of the nanotube support and anatase/rutile phase transformation.

According to the results of the photocatalytic study of the synthesized nanocomposites, the highest activity was obtained for TiO_2/o-MWCNT. The optimal ratio used for the synthesis of TiO_2/o-MWCNT was also applied for the preparation of all other nanocomposites (160 mg MWCNT, 13.6 cm^3 2-propanol and 4 cm^3 Ti(*iso*-$OC_3H_7)_4$: $[MWCNTs]_{loading} = 12.9$ wt%). Higher multi-wall carbon nanotubes (MWCNTs) loadings led to increased shielding of the active photocatalytic sites and increased absorbance and scattering of photons, which caused a decrease in the photocatalytic activity.

3.1. Boehm analysis

In order to optimize the properties of the surface of carbon nanotubes in a nanocomposite, *i.e.*, charge transfer at the nanomaterial interface, it was necessary to study the influence

Table 1
Results of the Boehm titration[a] of the raw and functionalized MWCNT.

	Carboxyls	Lactones	Phenols	Total acidic sites	Total basic sites
MWCNT (raw-MWCNT)	0.07	0.28	0.24	0.58	0.19
o-MWCNT	0.87	1.78	1.43	4.09	0.42
e-MWCNT	0.15	1.24	1.83	3.22	1.15
p-MWCNT	0.18	1.32	1.70	3.15	1.04

[a]In mmol/g.

of the introduction of different types of functional groups on the photocatalytic activity. The functionalization method of the raw-MWCNT caused the introduction of different types, quantities and distribution of the functional groups, which contribute significantly to the type and strength of chemical bonding of TiO_2 onto the CNT surface and thus the effectiveness of the charge transfer properties through the TiO_2/modified MWCNT interface. Oxidative treatment of MWCNT caused degradation of the graphitic structure, mainly at the nanotube ends, and graphitic plane opening created sidewall defect sites thereby introducing oxygen functionalities. Subsequent reaction with EDA or PDA introduced amino-terminated functional groups which were quantified from the results of Boehm titration data (Table 1). The applied mild and efficient coupling method for amino functionalization provided a high extent of transformation of carboxylic groups to amide groups containing free amino terminal functionalities.

3.2. Textural analysis

Specific surface area (S_p) and pore volume (V_p) of the raw-, o- and amino-functionalized MWCNT, as well as corresponding nanocomposites and pure TiO_2 are given in Table 2. Largest surface area, S_p, was found for the raw-MWCNT, while the value was significantly decreased for o-MWCNT. The decrease in the surface area and pore volumes were probably due to the smaller confined space between the o-MWCNT [19], and the introduction of oxygen-containing functional groups [8], which contributed to the decrease of the effective MWCNT surface. Modification with EDA and PDA resulted in increases in S_p and V_p. This could be explained if interparticle repulsions between e-MWCNT and p-MWCNT resulted in smaller-sized "globs" of MWCNT and/or if the additional ultrasound treatment used during amino-functionalization resulted in smaller aggregates of e-MWCNT and p-MWCNT [16]. Additionally, the surface area and pore volume of pure TiO_2 was low (Table 2), which is additional evidence that TiO_2 precipitation caused the decreases in S_p and V_p of all the nanocomposites.

3.3. FTIR analysis

Analysis of the FTIR spectra of the investigated samples proved itself to be a useful tool for obtaining information about

Table 2
Specific surface area (S_p) and pore volume (V_p) of the raw-, o-, e-, and p-MWCNT, as well as the synthesized nanocomposites and pure TiO_2.

Sample	S_p ($m^2\ g^{-1}$)	V_p ($cm^3\ g^{-1}$)
TiO_2–Blank	17.44	0.048
MWCNT (raw-MWCNT)[a]	187.58	0.755
o-MWCNT[a]	78.49	0.328
e-MWCNT[a]	101.24	0.538
p-MWCNT	108.42	0.581
TiO_2/o-MWCNT	66.25	0.081
TiO_2/e-MWCNT	59.15	0.072
TiO_2/p-MWCNT	57.02	0.069

[a]Ref. [16].

the interaction of the MWCNT supports and the deposited TiO_2 photoactive material (Fig. 2). FTIR analysis of the synthesized nanocomposites was performed to obtain qualitative estimations of the presence of residual functional groups after TiO_2 precipitation. The differences in the FTIR spectra of the modified MWCNT and the nanocomposite materials were analyzed by the differences in the peak intensity, peak shifting and peak appearance or disappearance, which is an indication of the degree of interaction of the functional groups and the TiO_2 deposits. Changes in the interaction of the groups resulted in bond strength changes, which resulted in changes in the vibration frequencies *i.e.*, changes in the wavelength values. Band shifts to lower or higher frequencies indicates bond weakening or strengthening, respectively.

The bands observed at $\approx 3400\ cm^{-1}$ and $\approx 1650\ cm^{-1}$ were assigned to the stretching and deformation vibrations of the OH groups present at the TiO_2 surface and from adsorbed water, respectively. The former arises from partial hydrolysis during synthesis and moisture adsorption from the air. Additionally, the absorption bands in the region from 1000 to 500 cm^{-1} correspond to Ti–O bond vibrations in the TiO_2. Generally, it could be stated that synthesis of TiO_2 nanocomposite provided a method for TiO_2 deposition covering most of the functional groups present at the o-, e- and p-MWCNT surfaces. The most intimate contact of two phases was achieved in the TiO_2/o-MWCNT nanocomposite, while analysis of FTIR spectra of TiO_2/e- and TiO_2/p-MWCNT photocatalysts indicated that differences in the reactivity of the alkyl (higher) and aromatic (lower) amino groups governed the contribution of either TiO_2 nanoparticles formation bonded

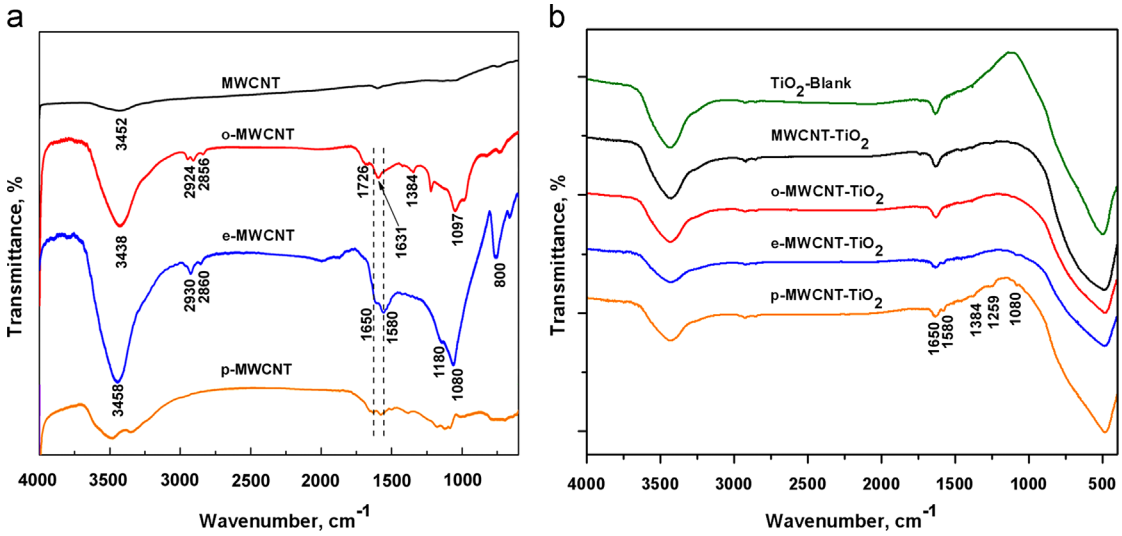

Fig. 2. FTIR spectra of the raw-, o-, e- and p-MWCNT (a); and synthesized nanocomposite photocatalysts (b).

to MWCNT surface or homogeneous nucleation in solution. The FTIR spectra of the TiO_2/e- and TiO_2/p-MWCNT photocatalysts clearly showed that the higher reactivity of the amino-alkyl group resulted in a more homogeneous deposition of TiO_2, *i.e.*, drive preferentially the reaction at the MWCNT surface and thus more nucleation center were formed and the subsequent crystallization (crystal growth) produced a more homogeneous covering. Lower reactivity and probably lower compatibility of aromatic moieties with the TiO_2 deposit contributed to the creation of larger non-bonded TiO_2 grains and clusters with also an observable TiO_2 deposit at the p-MWCNT surface (Fig. 4).

3.4. XRD analysis

Phase composition, crystallite size, structural and surface properties of the obtained TiO_2/MWCNT nanocomposites were analyzed according to the XRD (Fig. 3) and TEM/HRTEM results (Fig. 5). Powder X-ray diffraction (XRD) patterns of the synthesized nanocomposite photocatalysts are presented in Fig. 3. Studies of the crystalline structure showed that pure anatase TiO_2 phase was present in the nanocomposites and the pure TiO_2.

The mean crystallite size of TiO_2 nanoparticles (Table 3) decorating the raw-, oxidized and amino functionalized MWCNT surfaces were calculated using the Scherrer Equation based on the full-width-at-half-maximum-height of the characteristic peak in the corresponding XRD patterns (Fig. 3). A somewhat smaller crystallite size was found for TiO_2/o-MWCNT, indicating that more reactive centers were accessible for coordination, while the introduction of aminoethyl and aminophenyl bridging groups diminished the numbers of the available reactive centers.

The results given in Table 3 indicate a slight dependence of the mean crystallite size on the method of modification of the MWCNT.

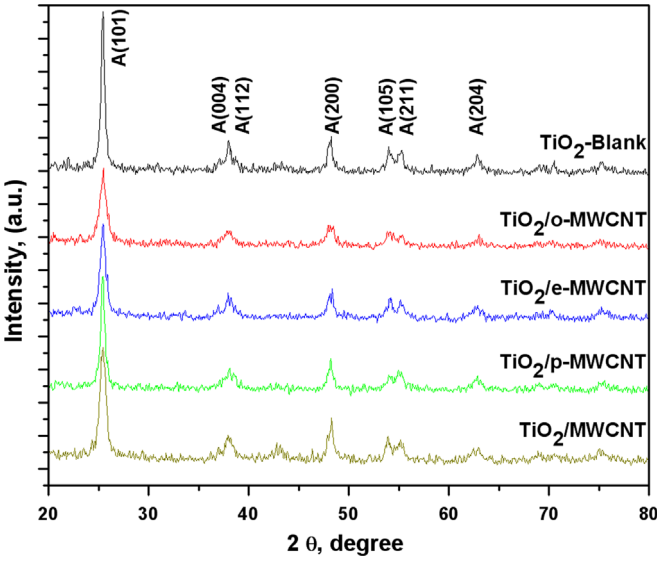

Fig. 3. XRD patterns of the synthesized photocatalysts.

Table 3
The mean crystallite size of the anatase nanoparticles.

Sample	D_{mean} (nm)
TiO_2–Blank	16.2 ± 0.9
TiO_2/MWCNT	14.5 ± 0.8
TiO_2/o-MWCNT	12.1 ± 0.3
TiO_2/e-MWCNT	13.3 ± 0.5
TiO_2/p-MWCNT	13.5 ± 0.7

3.5. SEM analysis

FEG-SEM images of the samples obtained by precipitation of TiO_2 onto raw-, o-, e- and p-MWCNT supports are shown in Fig. 4.

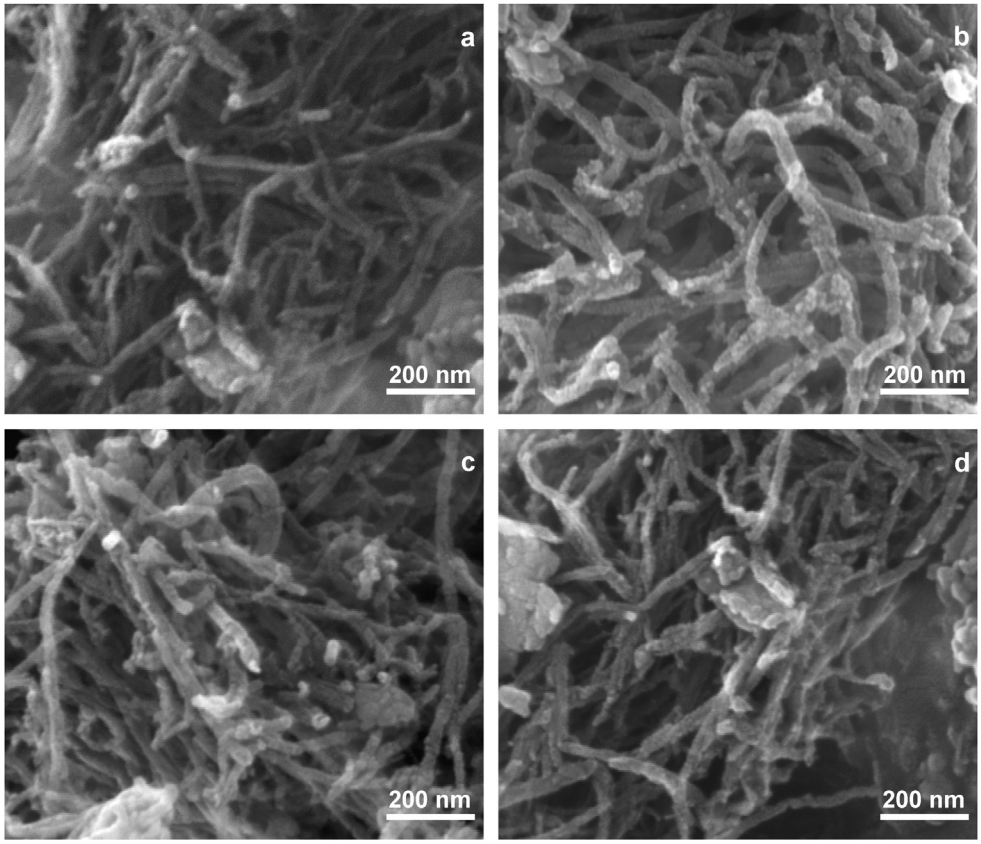

Fig. 4. FEG-SEM images of (a) TiO_2/MWCNT; (b) TiO_2/o-MWCNT; (c) TiO_2/e-MWCNT, and (d) TiO_2/p-MWCNT photocatalysts.

The treatment of o-MWCNT with Ti(*iso*-$OC_3H_7)_4$ resulted in a more uniform precipitation of titania, leading to tubes with a population of small observable prominences more or less uniformly distributed on the surface of the nanotubes. Compared with those of TiO_2/o-MWCNT, the sidewalls of TiO_2/e- and p-MWCNT are more corrugated and larger aggregates of bonded TiO_2 are detectable with increased diameter at domains where a significant numbers of functional groups were located. The largest noticeable distinct phase of titania, with embedded raw-MWCNT, was found for TiO_2/MWCNT (Fig. 4a), indicating very low bonding specificity of the non-modified MWCNT surface, which is mostly a graphitic, non-polar surface, toward the titania precursor.

The FEG-SEM micrographs revealed that TiO_2/o-MWCNT (Fig. 4b), compared to TiO_2/amino-modified MWCNT (Fig. 4c and d), had a more homogeneous and thicker TiO_2 coating. The larger diameter of the observable pure TiO_2 nanoparticles and clusters obtained for TiO_2/e- and TiO_2/p-MWCNT indicated lower affinities of the titania precursor for the surface of the amino-modified nanotube supports. A study of the different reaction condition, e.g., the presence of water, even at ppm quantity in reaction mixture, caused the formation of larger titania clusters, bonded and non-bonded to the MWCNT support. After sonication, the intimate coatings on the MWCNT surfaces were stable after prolonged time of exposure, but the non-bonded aggregates were easily broken away becoming free standing particulates. From these results, it could be assumed that the titania nanoparticles at the MWCNT surface were bonded by Ti–O(O)C/Ti–OC (carboxylic/phenolic) and Ti–NHRNH(O)C (R is ethyl or phenyl) bonds in TiO_2/o-MWCNT and TiO_2/amino modified-MWCNT nanocomposite, respectively.

3.6. TEM/HRTEM analysis

TEM/HRTEM analysis was applied in order to study the morphologies of the obtained nanocomposites, *i.e.*, the interaction of the TiO_2 deposits and the functional groups at the surface of the modified MWCNT. As an example, the obtained results are given for TiO_2/o-MWCNT in Fig. 5. The high resolution images (Fig. 5b) shows clearly the presence of TiO_2 nanocrystals on the surfaces of the o-MWCNT. The HRTEM images (Fig. 5b and c) indicate intimate contact between the MWCNT surface and randomly orientated TiO_2 nanocrystals. It could be also observed that, except for the nanoparticle directly bonded to the MWCNT surface, randomly distributed larger aggregates of TiO_2 exist in Fig. 5a. The lateral binding of the TiO_2 aggregates and nanoparticles present at the MWCNT surface create weak connections to the MWCNT support (Fig. 5a). The electron energy-loss spectrum-EELS (insets in Fig. 5b and c) clearly show the presence of Ti L_{23} edges at 450 eV and O K edges at 530 eV, indicating pure TiO_2 nanocrystals.

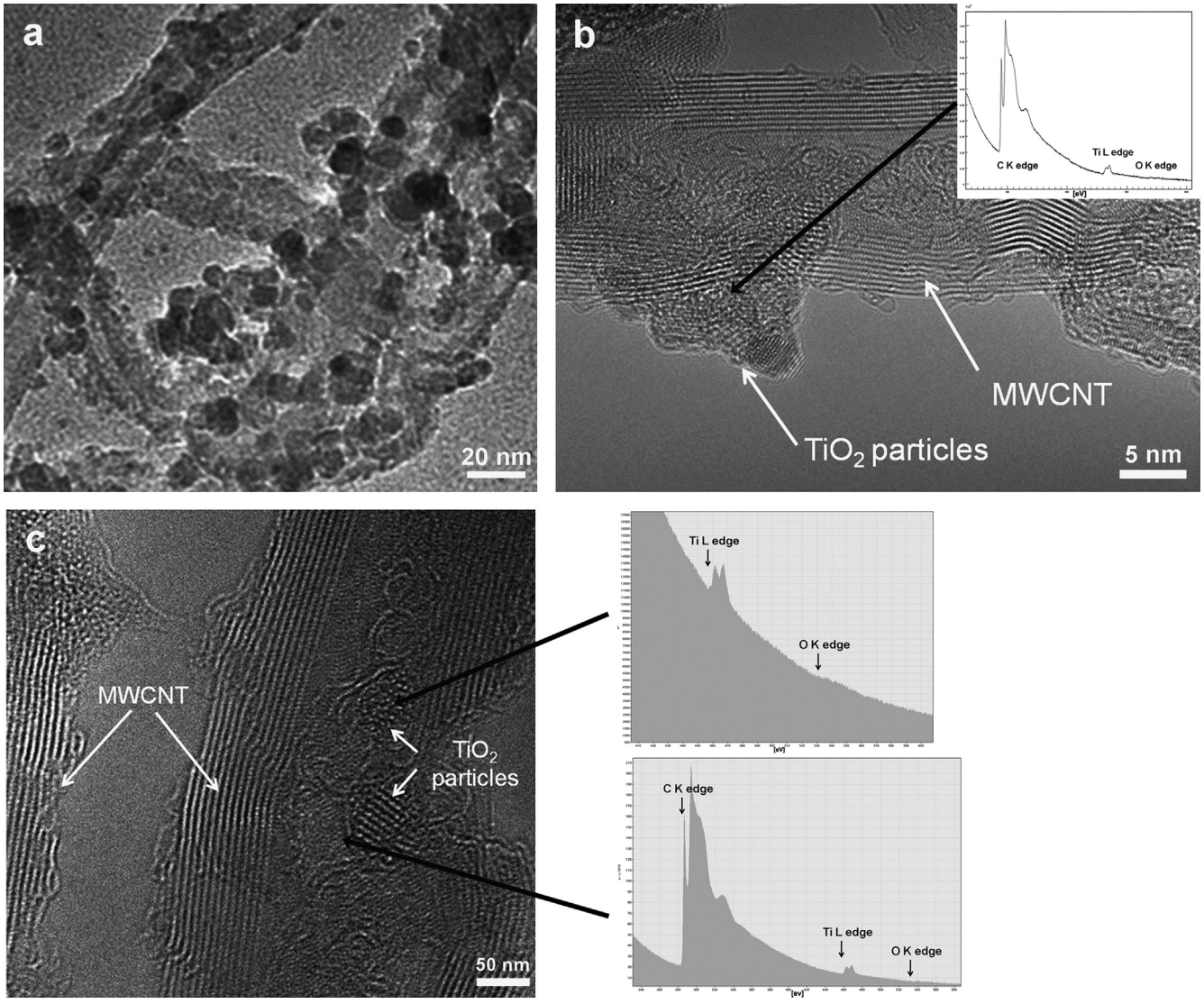

Fig. 5. TEM/HRTEM images of TiO_2/o-MWCNT nanocomposite: (a) TEM image of nanocomposite; (b and c) HRTEM images with TiO_2 nanoparticles, marked by arrows, present on surface of o-MWCNT; EELS of TiO_2 crystallites – inset in (b and c).

The structural changes of the MWCNT surface due to oxidation, *i.e.*, the introduction of oxygen containing functionalities, create plane structures and MWCNT end opening, which then becomes highly vulnerable sites for additional oxidative attack. Further oxidative attack at the formed defects favors the formation of cluster defects rather than a random distribution along the MWCNT. The defect sites behave as adhesive centers that result in concentrations of degradation processes within limited domains and hence, the oxidative process causes penetration into the inner layers of the MWCNT [20]. The primary binding sites, *i.e.*, the oxygen-containing functionalities, are nucleation centers for crystal growth of TiO_2 at the o-MWCNT surface, and crystallization, grain growth and crystal growth inside mesopores (Fig. 5b). Homogenous nucleation in solution provides crystallization centers that are subjected to crystal growth and coarsening, *i.e.*, lateral binding, resulting in the formation of large aggregates of TiO_2 nanoparticles. The reactivity of Ti(*iso*-$OC_3H_7)_4$ with moisture is an important factor which governs the hydrolysis of the titania precursor, providing conditions for either homogeneous nucleation in solution or heterogeneous nucleation on the MWCNT surface. In this study, the mildest hydrolytic method was applied to direct nano-TiO_2 precipitation onto the modified MWCNT surfaces by favoring competitive reactions between either moisture (water hydroxyl group) or hydroxyl and carboxyl groups (o-MWCNT) or amino functionalities (e- and p-MWCNT) at surface support. According to the presented results the most convenient competitiveness between the reactivity of moisture and groups on the modified MWCNT surface was achieved in the case of o-MWCNT. Besides the optimization of the synthesis procedure presented in this work, it was shown that the higher reactivity of titania precursor $TiBr_4$, in comparison to Ti(*iso*-$OC_3H_7)_4$, with the oxygen containing surface functionalities provided higher photocatalytic activities of the synthesized nanocomposite photocatalysts [13].

3.7. Photocatalytic study

The efficiencies of all the synthesized photocatalysts in the photocatalytic degradation of the chosen dye are shown in Fig. 6. Photolysis of the dye in the absence of a photocatalyst showed negligible time-dependent changes in the dye concentration and the amount of degraded dye was 1% after 6 h (Fig. 6). Low activity was found in the presence of pure TiO_2 (TiO_2–Blank), *i.e.*, 3% of initial dye still remained in solution after 6 h of irradiation. However, the TiO_2/MWCNT hybrid samples exhibits higher photocatalytic degradation efficiency; the highest value was obtained for TiO_2/o-MWCNT (47 min), while TiO_2/e-MWCNT (84 min) and TiO_2/p-MWCNT (98 min) exhibited somewhat lower activities.

Efficient application of titania nanocomposite demands well-dispersed photocatalyst nanoparticles, *i.e.*, the availability of surface active sites at the particle/solution interface. Such behavior depends on catalyst morphology: particle size and surface area, as well as on inter-particle interaction. It is worth mentioning that the TiO_2/o-, TiO_2/e- and TiO_2/p-MWCNT samples displayed very good photocatalytic efficiency for CI RO 16 degradation, which implies that MWCNT support contributed to an enhancement of the photocatalysis. Three contributing factors are important: adsorption of the dye molecules, light absorption, and an effective charge separation and transportation process [13]. Many studies revealed that dye adsorption on MWCNT arise from two contributing factors: physical adsorption and π–π interaction of the hydrophobic part of the sorbate and the intact graphene plane present at the surface of MWCNT [21]. It was found that the adsorptive capabilities of the nanocrystalline TiO_2 was not a main factor controlling the photocatalytic activity [22] as although surface hybridization of TiO_2 with graphite-like carbon improved the photocatalytic efficiency, only a small improvement in the adsorption properties was registered [23]. The photocatalytic activity of graphene-supported TiO_2 was almost independent of the specific surface area, while the life-time of the photogenerated electron/hole pairs was found to be the main factor influencing the photocatalytic efficiency [24].

Similarly, the results of specific surface area and pore volume (Table 2) and photocatalytic studies (Fig. 6) of the synthesized photocatalysts indicated that the textural parameters are a contributing factor that improved the photocatalytic efficiencies. A comparison of the photocatalytic activities of all the nanocomposites and pure TiO_2 indicated that efficient separation of the photogenerated electron/hole is the main factor contributing to an increased photocatalytic activity (Fig. 7). According to a previous study, the MWCNT support contributes to more effective charge separation and suppression of electron/hole pair recombination [13]. Hybridizing both raw and modified MWCNT with a grafted inorganic nanostructure, TiO_2, resulted in photocatalysts of improved charge transfer properties, which helps in reducing electron-hole recombination (Fig. 7). The oxygen-containing and amino-terminated functionalities at the TiO_2/o-, e- and p-MWCNT interface, respectively, supports the electron transporting properties, *i.e.*, the migration efficiency of the photogenerated electrons, and these processes depends on the total acidity (the acidic functional groups present in o-MWCNT) and the type of amino functionalities present at the e- and p-MWCNT surfaces (Table 1).

The dye degradation rate obtained using TiO_2/o-MWCNT was higher than for all other nanocomposites and pure TiO_2, which indicates the great significance of oxygen-containing functionalities at the MWCNT surface on the photocatalytic activity, *i.e.*, their electron transporting properties. Additionally, the low photocatalytic activity of pure TiO_2 indicates that the amino modified-MWCNT in TiO_2/e- and p-MWCNT also contributed to enhanced photocatalytic activities. The MWCNT could act as electron sinks, *i.e.*, the photogenerated electrons are transferred into the MWCNT providing a low probability of the recombination process. The large electron-storage capacity of the MWCNT is the driving force for the

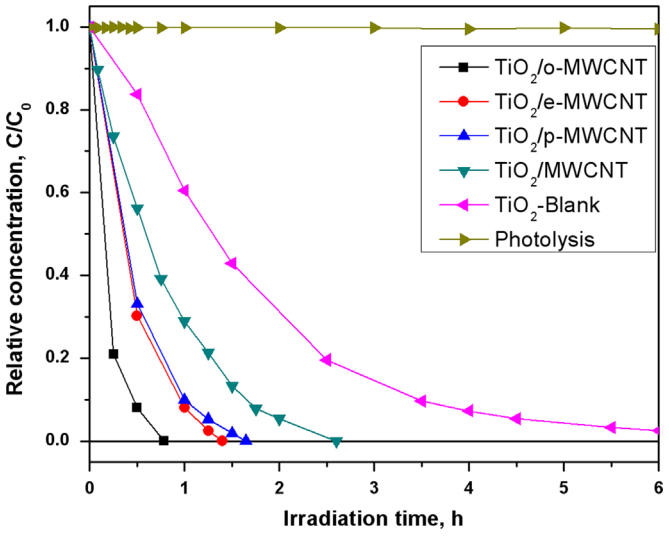

Fig. 6. Relative dye concentration change vs. irradiation time in the presence of the synthesized photocatalysts.

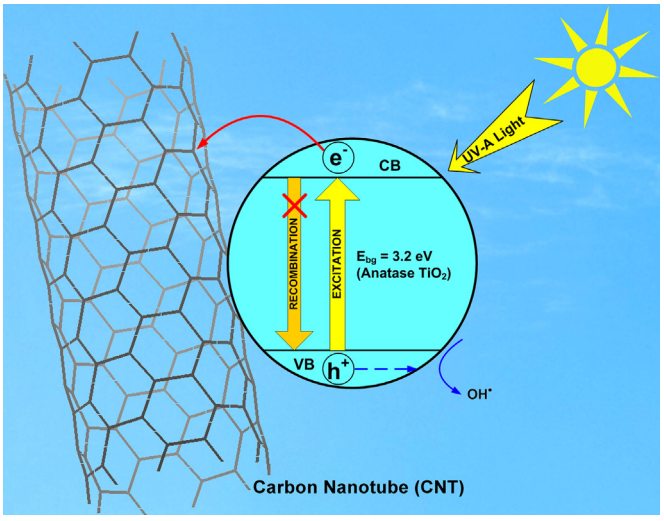

Fig. 7. The simplified mechanism for the enhanced photocatalytic activity of TiO_2/CNT nanocomposite catalyst.

capture of photon-excited electrons from the conduction band of the TiO_2. Otherwise, the MWCNT could act as impurities through Ti–O(O)C/Ti–OC and Ti–NHRNH(O)C bonds, which contribute to efficient electron/hole separation. Simultaneously, MWCNT could provide fast conduction of the captured photon-excited electrons, hindering thereby the recombination of electron-hole pairs. Moreover, the TiO_2/MWCNT systems may be more complex as the contribution of two distinct effects was recognized: the first, extended light absorption due to the presence of C–O–Ti bonds, similar to those in carbon-doped TiO_2, and the second addresses the electronic configuration of the CNT that consists of large numbers of mid band-gap states introduced by the existing defects, which aids electronic excitation [4,6].

Moreover, recently a DFT study on the electronic structure of semiconducting and metallic tubes in TiO_2/CNT heterojunctions showed that the photogenerated electron, injected into the conduction band of TiO_2, effectively reduced the transition energy, which contributed to an enhancement of the phototactivity. Additionally, the DFT simulations evidenced that the higher visible light, compared to ultraviolent irradiation, induced photocatalytic activity of CNT/TiO_2 hybrid materials of semiconducting, contrasted with metallic CNT/TiO_2 systems, was due to efficient charge separation across the interface [25].

The advantageous application of the selected catalysts is justified by their prolonged use, *i.e.*, long-term reusability, in the course of consecutive cycles of catalyst application for dye photodegradation. The reusability study showed that the photodegradation efficiency of all the synthesized photocatalysts were almost preserved in five consecutive experiments, *i.e.*, the overall decreases in efficiency were in the range 3–9% of the initial values, indicating good catalyst recovery in the purification process applied in a previous study [13]. From the practical point of view, such results indicate the feasibility of efficient application and reusability of the catalysts, which could be a good basis for the development and practical application of the obtained photocatalysts in environmental clean-up.

4. Conclusions

Improved photocatalytic performance of the synthesized nanocomposite photocatalysts was obtained by a sol–gel process, *i.e.*, the hydrolysis of Ti(*iso*-$OC_3H_7)_4$ to provide TiO_2 growth on the surface of differently functionalized MWCNT. Oxidation and subsequent amino-functionalization of MWCNT introduced significant amounts of functional groups, which play an important role in the nucleation and binding of TiO_2, as well as contributing to differences in photocatalytic activities of the synthesized nanocomposites. Additionally, the presented processes resulted in pure anatase phase TiO_2 nanoparticles chemically bonded to the surface of TiO_2/modified-MWCNT. The highest UV-A induced activity was found for TiO_2/o-MWCNT and somewhat lower values for TiO2/e-MWCNT and TiO_2/p-MWCNT photocatalysts, indicating that the enhancement of photocatalysis was supported by the effective electron transfer properties of oxygen-containing functional groups that support efficient charge transportation and separation of the photogenerated electron-hole pairs. The amino functional groups were somewhat less effective.

Acknowledgments

Financial support through the Ministry of Education, Science and Technological Development of the Republic of Serbia, Project no. III 45019, is gratefully acknowledged. V.R. R. acknowledges the support of the Nanotechnology and Functional Materials Center, funded by the European FP7 Project no. 245916, from the Ministry of Education, Science and Technological Development of the Republic of Serbia, Project no. 172054. Quantitative high resolution electron microscopy analysis was performed at the National Center for Electron Microscopy, Lawrence Berkeley National Laboratory, funded by the U.S. Department of Energy under Contract DE-AC02-05CH11231.

References

[1] A. Fujishima, X. Zhang, D.A. Tryk, TiO_2 photocatalysis and related surface phenomena, Surface Science Reports 63 (2008) 515–582.
[2] A. Fujishima, K. Honda, Electrochemical photolysis of water at a semiconductor electrode, Nature 238 (1972) 37–38.
[3] N. Ruzycki, G.S. Herman, L.A. Boatner, U. Diebold, Scanning tunneling microscopy study of the anatase (100) surface, Surface Science Letters 529 (2003) 239–244.
[4] K. Woan, G. Pyrgiotakis, W. Sigmund, Photocatalytic carbon-nanotube–TiO_2 composites, Advanced Materials 21 (2009) 2233–2239.
[5] G. Socol, Yu. Gnatyuk, N. Stefan, N. Smirnova, V. Djokić, C. Sutan, V. Malinovschi, A. Stanculescu, O. Korduban, I.N. Mihailescu, Photocatalytic activity of pulsed laser deposited TiO_2 thin films in N_2, O_2 and CH_4, Thin Solid Films 518 (2010) 4648–4653.
[6] R. Leary, A. Westwood, Carbonaceous nanomaterials for the enhancement of TiO_2 photocatalysis, Carbon 49 (2011) 741–772.
[7] K. Ouyang, S. Xie, X. Ma, Photocatalytic activity of TiO2 supported on multi-walled carbon nanotubes, Ceramics International 39 (2013) 7531–7536.
[8] K.A. Wepasnick, B.A. Smith, K.E. Schrote, H.K. Wilson, S. R. Diegelman, D.H. Fairbrother, Surface and structural characterization of multi-walled carbon nanotubes following different oxidative treatments, Carbon 49 (2011) 24–36.
[9] S. Banerjee, T. Hemraj-Benny, S.S. Wong, Covalent surface chemistry of single-walled carbon nanotubes, Advanced Materials 17 (2005) 17–29.
[10] D. Tasis, N. Tagmatarchis, A. Bianco, M. Prato, Chemistry of carbon nanotubes, Chemical Reviews 106 (2006) 1105–1136.
[11] D. Eder, Carbon nanotube-inorganic hybrids, Chemical Reviews 110 (2010) 1348–1385.
[12] G. Jiang, X. Zheng, Y. Wang, T. Li, X. Sun, Photo-degradation of Methylene Blue by multi-walled carbon nanotubes/TiO_2 composites, Powder Technology 207 (2011) 465–469.
[13] V.R. Djokić, A.D. Marinković, M. Mitrić, P.S. Uskoković, R.D. Petrović, V.R. Radmilović, Dj.T. Janaćković, Preparation of TiO_2/carbon nanotubes photocatalysts: The influence of the method of oxidation of the carbon nanotubes on the photocatalytic activity of the nanocomposites, Ceramics International 38 (2012) 6123–6129.
[14] G. Vuković, A. Marinković, M. Obradović, V. Radmilović, M. Čolić, R. Aleksić, P.S. Uskoković, Synthesis, characterization and cytotoxicity of surface amino-functionalized water-dispersible multi-walled carbon nanotubes, Applied Surface Science 255 (2009) 8067–8075.
[15] M.D. Obradović, G.D. Vuković, S.I. Stevanović, V.V. Panić, P.S. Uskoković, A. Kowal, S.Lj. Gojković, A comparative study of the electrochemical properties of carbon nanotubes and carbon black, Journal of Electroanalytical Chemistry 634 (2009) 22–30.

[16] G.D. Vuković, A.D. Marinković, M. Čolić, M.Đ. Ristić, R. Aleksić, A. A. Perić-Grujić, P.S. Uskoković, Removal of cadmium from aqueous solutions by oxidized and ethylenediamine-functionalized multi-walled carbon nanotubes, Chemical Engineering Journal 157 (2010) 238–248.
[17] B.W. Smith, D.E. Luzzi, Electron irradiation effects in single wall carbon nanotubes, Journal of Applied Physics 90 (2001) 3509–3606.
[18] H.P. Boehm, in: D.D. Eley, H. Pines, P.B. Weisz (Eds.), Advances in Catalysis, Vol. 16, Academic Press, New York, 1966, pp. 179–274.
[19] C. Lu, C. Chiu, Adsorption of zinc(II) from water with purified carbon nanotubes, Chemical Engineering Science 61 (2006) 1138–1145.
[20] N. Lachman, X. Sui, T. Bendikov, H. Cohen, H. Daniel Wagner, Electronic and mechanical degradation of oxidized CNTs, Carbon 50 (2012) 1734–1739.
[21] J. Ma, R. Xiao, J. Li, J. Yu, Y. Zhang, L. Chen, Determination of 16 polycyclic aromatic hydrocarbons in environmental water samples by solid-phase extraction using multi-walled carbon nanotubes as adsorbent coupled with gas chromatography–mass spectrometry, Journal of Chromatography A 1217 (2010) 5462–5469.
[22] M. Yan, F. Chen, J. Zhang, M. Anpo, Preparation of controllable crystalline titania and study on the photocatalytic properties, Journal of Physical Chemistry B 109 (2005) 8673–8678.
[23] L.W. Zhang, H.B. Fu, Y.F. Zhu, Efficient TiO_2 photocatalysts from surface hybridization of TiO_2 particles with graphite-like carbon, Advanced Functional Materials 18 (2008) 2180–2189.
[24] Y. Zhang, Z.-R. Tang, X. Fu, Y.-J. Xu, Engineering the unique 2D mat of graphene to achieve graphene–TiO_2 nanocomposite for photocatalytic selective transformation: what advantage does graphene have over its forebear carbon nanotube?, ACS Nano 5 (2011) 7426–7435.
[25] R. Long, Electronic structure of semiconducting and metallic tubes in TiO_2/Carbon nanotube heterojunctions: density functional theory calculations, Journal of Physical Chemistry Letters 4 (2013) 1340–1346.